Final-state distribution for $Na(3P_J)+Na(3P_{J'})\rightarrow Na(nL_{J''})+Na(3S_{1/2})$ collisional excitation transfer

Steven A. Davidson,* J. F. Kelly, and A. Gallagher†
Joint Institute for Laboratory Astrophysics, University of Colorado and National Bureau of Standards, Boulder, Colorado 80309
(Received 31 December 1985)

We report the ratio of rate coefficients for the excitation-transfer reaction $Na(3P_J)+Na(3P_{J'})\rightarrow Na(nL_{J''})+Na(3S_{1/2})$, which has sometimes been labeled energy pooling, measured in a cell at $T=640$ K. Rate-coefficient ratios are given for $nL_{J''}=4D_{3/2}$, $4D_{5/2}$, $4F_{5/2}$, $4F_{7/2}$, and $5S_{1/2}$, each for $J=J'=1/2$ and 3/2. We also report the $nL_{J''}$ ratios when the $3P$ states are populated in nearly statistical ratios; these are related to the rate coefficients when $J=1/2$ and $J'=3/2$.

I. INTRODUCTION

The excitation-transfer process in which a collision between two sodium atoms excited to the $3P$ state results in formation of a highly excited atom and a ground-state atom has been known for some time.[1] The absolute rate coefficient for the excitation transfer to $4D$ and $5S$ states has been measured in several laboratories,[2–6] and relative good agreement ($\sim 30\%$) exists between two of the more recent measurements.[2,3] This type of excitation-transfer process has also been observed,[7,8] measured,[9–11] and calculated[12] for other alkali metals. None of the measurements made with sodium have taken into account the dependence on the J values of the $3P$ reactants, nor do they determine the product state's J value. Only Refs. 6 and 13 consider excitation transfer to other states adjacent in energy to the $4D$ and $5S$ states. Here we report relative measurements of the rate coefficients for producing the energetically nearby $5S_{1/2}$, $4D_{3/2}$, $4D_{5/2}$, $4F_{5/2}$, and $4F_{7/2}$ states from the different combinations of $Na(3P_J)+Na(3P_{J'})$ collisions (see Figs. 1 and 2).

The process can be represented as

$$Na(3P_J)+Na(3P_{J'}) \xrightarrow{k_{nL_{J''}}^{(J,J')}} Na(nL_{J''})+Na(3S_{1/2}) . \quad (1)$$

This process is sometimes described as a pooling of energy[4,9] among the colliding species, but it is a form of atom-atom electronic energy transfer and can be described in the same manner as the more familiar $A^*+B\rightarrow A+B^*$ and $A+B^*\rightarrow A^*+B$ processes. For thermal (slow) collisions the interaction between the atoms is well characterized by the molecular adiabatic potentials, with nonadiabatic energy transfer generally occurring at "avoided crossings."[14,15] In particular, process (1) is best described in terms of the formation of an excited diatomic molecule Na_2^* and its subsequent dissociation into excited- and ground-state atoms, as described in Refs. 16–19 and 13 (see Fig. 1).

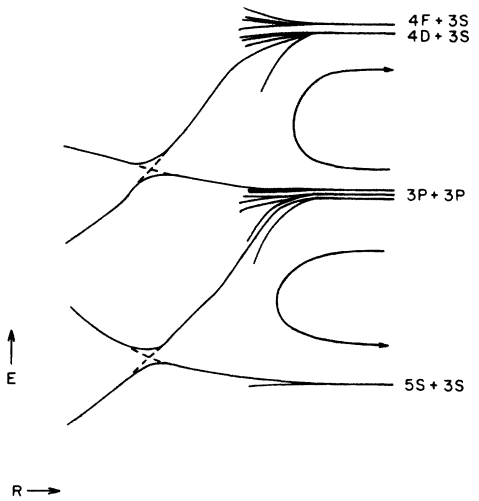

FIG. 1. Diagrammatic representation of the potentials for Na_2 states in the region of interest for these experiments. Shown here are a few of the dozens of potentials, due to fine structure, and two representative adiabatic level crossings.

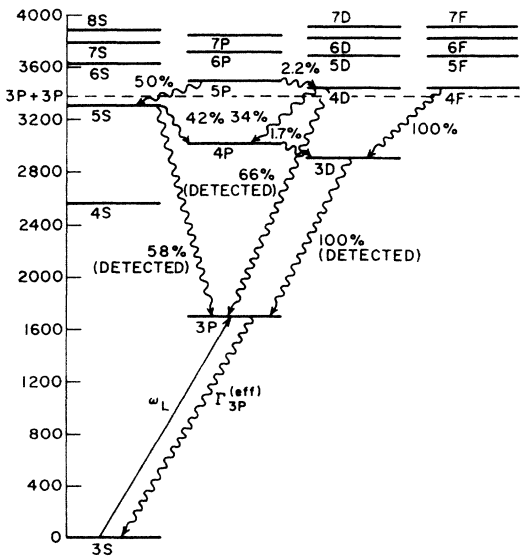

FIG. 2. Pumping, cascade branching, and detection scheme for steps (1) and (2). For step (3) only $4D$-$3P$ light was detected.

We believe that the detailed set of rate coefficients reported here provide a very stringent test of theories, such as those of Kowalczyk[16–18] and Henriet *et al.*[19] for the shape and crossing parameters of potential curves of the Na_2 system. These rate coefficients are also relevant to pumping mechanisms for ir laser transitions between highly excited states of sodium,[20,21] and may be useful in studies of multistep ionization processes in excited sodium vapor.[22–27]

The method we used to measure the rate-coefficient ratios was to optically excite sodium atoms in a cell to one of the Na($3P_J$) states and measure fluorescence intensities from the $nL_{J''}$ states that are produced by reaction (1) (see Fig. 2). In order to minimize secondary processes such as multiphoton ionization, electron collisions, and other higher-order processes,[22,26,28,29] a relatively diffuse ($\sim$1 cm diameter), weak ($\sim$50 mW) cw laser beam was used. In order to obtain good signal-to-noise levels the cell was operated at relatively high sodium densities, and therefore with high resonance-line optical depth. The resulting resonance-line radiation trapping improved the signal level due to the longer effective lifetime of the $3P$ state, which increased the population of Na($3P$). When properly accounted for, the effects of this radiation trapping cause no significant systematic errors. We avoided some of the common difficulties of using optically thick vapor by measuring fluorescence-intensity ratios, which eliminated the dependence of our results on the spatial distribution of Na($3P$) atoms. The radiation trapping also serves to scramble the polarization of the exciting laser light (by repeated absorptions and reemissions) so that there is no M_J-level selectivity.

II. THE EXPERIMENT

The experiment was carried out in a cell (see Fig. 3) consisting of a 5-cm cube of stainless steel drilled out to make a cross and vacuum sealed with metal O rings to sapphire windows.[30] Sapphire rods were inserted along one axis of the cross to limit the excitation to a 6.3-mm-deep viewable region. Apertures were placed on both sides of the rods to minimize collection of scattered light from, and the broadband fluorescence of, the rods. As the rods have a 12.5 mm diameter, this produces an approximation to an infinite slab geometry between the rods (see Fig. 3). The cell was contained in a firebrick oven with quartz windows to maintain a uniform temperature of $\sim$640 K. The sodium density [Na] was controlled separately by adjusting the temperature of a sidearm within the range 470—570 K. Although the accuracy of the experiment does not depend critically on sodium density, we used and reconfirmed the vapor-pressure results of Huennekens.[30]

The $5S$ and $4D$ states branch $\sim\frac{2}{3}$ into visible transitions (616 and 578 nm—see Fig. 2) which can be detected by our photomultiplier, but the $4F$ state decays exclusively to the $3D$ state with 1.8-μm radiation. Only the $5S$, $4D$, and $4F$ states are expected to be significantly populated by process (1), and the $5S$ and $4D$ states branch less than 1% into $3D$, whereas the $4F$ state radiates 100% to $3D$. Thus, by detecting the $3D\rightarrow 3P$ fluorescence at

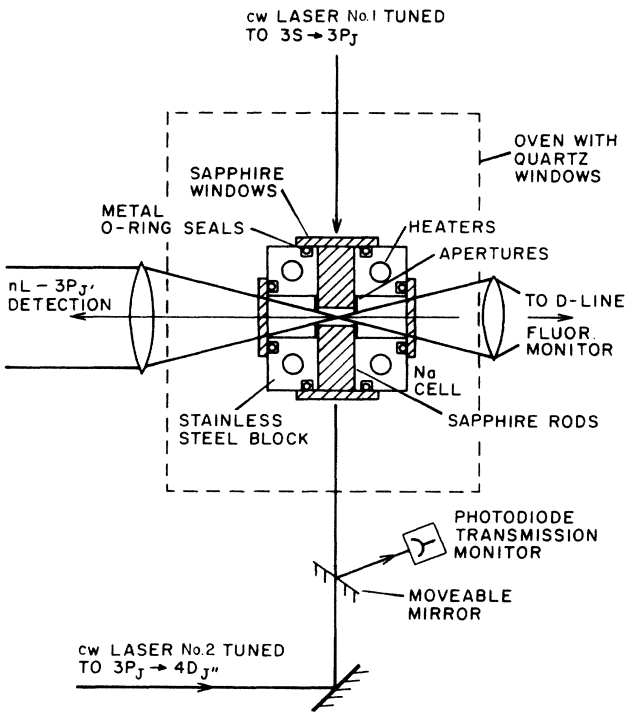

FIG. 3. Experimental setup. For steps (1) and (3), the $nL\rightarrow 3P_{J'}$ detection was by a 3/4-meter double monochromator and PMT, and laser no. 2 was not used. For step (2), the $4D$ fluorescence detection was through three interference filters ($\lambda\cong 5685$) to a PMT. All lenses were achromatic.

$\sim$820 nm and correcting for the slight contribution from the $5S$ and $4D$ states, the excitation transfer [Eq. (1)] to the $4F$ state is determined from the $3D$ fluorescence. The measured ratio of intensities from the $5S$, $4D$, and $3D$ fluorescence then yields ratios of rate coefficients. As already noted, we do not expect significant amounts of direct energy transfer to the $3D$ state by process (1), but if this occurs it is included in the rate coefficient we report for the $4F$ state.

Under our weak cw-excitation conditions, the fluorescence from the $5S$, $4D$, and $3D$ states is a factor of 10^5—10^7 weaker than the resonance-line fluorescence. Consequently, we used a 3/4-meter, double-grating monochromator with a red-sensitive photomultiplier to observe these fluorescences. The relative spectral sensitivity of the combination of light collection optics, monochromator, and photomultiplier tube (PMT) was calibrated by illuminating a white barium-sulfate-painted surface before and after the cell (testing for λ-dependent attenuation) with a calibrated tungsten iodide lamp. Since the lamp has a continuous spectrum and atomic lines are monochromatic, it is necessary to use the lamp intensity per wavelength interval and to multiply the observed experimental signal by the monochromator dispersion per unit wavelength interval at each wavelength (normally this is a minor correction). Achromatic lenses were used between the cell and monochromator to avoid introducing wavelength dependences to the imaging of the cell onto the monochromator. The spatial distribution of excited

atoms in the cell extended over a larger region than the spectrometer slit image, so that any slight residual imaging variations would not cause error.

The $nL_{J''}$ fine structure is below our spectral resolution, but each J'' state branches differently to the $3P_{1/2}$ and $3P_{3/2}$ states, and these two transitions are easily resolved by the monochromator. Therefore, we separately measured each $nL \rightarrow 3P_J$ transition, and from the intensity ratios we determined the J dependence of the $k_{nL_{J''}}$. In the case of $nL_{J''}=5S_{1/2}$, the intensity ratio must be 2:1, and provides an experimental check. Thus, spontaneous emission intensities of the $5S$ to $3P_{1/2}$ and $3P_{3/2}$ transitions (6161 and 6154 Å), the $4D$ to $3P_{1/2}$ and $3P_{3/2}$ transitions (5688 and 5686 Å), and the $3D$ to $3P_{1/2}$ and $3P_{3/2}$ transitions (8183 and 8195 Å) were measured.

Fifteen different $k_{nL_{J''}}(J,J')$ are of interest here: the initial state (J,J') combinations of (1/2,1/2), (1/2,3/2), and (3/2,3/2), and the final states $nL_{J''}=5S_{1/2}$, $4D_{3/2}$, $4D_{5/2}$, $4F_{5/2}$, and $4F_{7/2}$. The measurements of the ratios of these k values were done in three parts.

(1) First, at sufficiently low sodium densities, such that only the optically excited $3P_J$ state was significantly populated, we measured the ratios of $5S_{1/2}$, $4D_{J''}$, and $3D_{J''}$ fluorescence intensities with only $3P_{1/2}$ or only $3P_{3/2}$ excited. Thus, we obtained the five values of $k_{nL_{J''}}(1/2,1/2)$ relative to each other and the five values of $k_{nL_{J''}}(3/2,3/2)$ relative to each other.

(2) In the second part of the experiment, also at a relatively low [Na], we measured the ratio of Na($4D$) fluorescence intensity due to $\mathrm{Na}(3P_{1/2})+\mathrm{Na}(3P_{1/2})$ collisions versus that due to $\mathrm{Na}(3P_{3/2})+\mathrm{Na}(3P_{3/2})$ collisions. Here it was necessary to know the relative density of $\mathrm{Na}(3P_{1/2})$, when it was the only Na($3P$) species, versus the density of $\mathrm{Na}(3P_{3/2})$, when it was the only Na($3P$) species. These densities resulted from optical excitation along with radiation diffusion, and we used Holstein's theory of radiation diffusion[31] to calculate their ratio. This density ratio was also confirmed by measuring the $4D \rightarrow 3P$ fluorescence produced by absorbing light from a second cw laser tuned to $3P \rightarrow 4D$. Combining this result with that from part (1) yields the ratios of ten relative rate coefficients corresponding to $J=J'=1/2$ or 3/2.

(3) In the third part of the experiment, the Na density was raised until $\mathrm{Na}(3P_{3/2})+\mathrm{Na}(3S) \leftrightarrow \mathrm{Na}(3P_{1/2})+\mathrm{Na}(3S)$ excitation-transfer collisions produced a nearly equilibrated mixture[32] of $3P_J$-state population. Under these circumstances, $\sim\frac{4}{9}$ of the $\mathrm{Na}(3P)+\mathrm{Na}(3P)$ collisions are between one atom in the $3P_{1/2}$ and one in the $3P_{3/2}$ state. The four independent ratios of fluorescence intensity from the $5S_{1/2}$, $4D_{3/2,5/2}$, and $3D_{3/2,5/2}$ states have been measured under these conditions, providing four constraints on the five $k_{nL_{J''}}(1/2,3/2)$ relative to the set of ten k values from parts (1) and (2), i.e., the $k_{nL_{J''}}(1/2,3/2)$ are underdetermined by one parameter. Complete determination of the $k_{nL_{J''}}(1/2,3/2)$ could be done by measuring the four fluorescence-intensity ratios with sufficient accuracy for several ratios of $[\mathrm{Na}(3P_{1/2})]/[\mathrm{Na}(3P_{3/2})]$ also determined with great accuracy, but this was not done here, so we have incompletely determined the $k_{nL_{J''}}(1/2,3/2)$ ratios in this experiment.

The three experimental steps and their results will now be described in detail.

A. $k_{nL_{J''}}(1/2,1/2)$ and $k_{nL_{J''}}(3/2,3/2)$ data

In this part of the experiment, the density of sodium in the cell was maintained at 2.8×10^{12}, 6.4×10^{12}, or 1.6×10^{13} cm^{-3}, and the atoms were excited from the ground state ($3S_{1/2}$) to either the $3P_{1/2}$ or $3P_{3/2}$ state by radiation from a cw dye laser tuned to the wing of the resonance line. The resonance-line absorption cross section is $\sim5\times10^{-12}$ cm^2 for $3S \rightarrow 3P_{3/2}$ and $\sim2.5\times10^{-12}$ cm^2 for $3S \rightarrow 3P_{1/2}$, and the cell width is 0.63 cm so that the sodium vapor is optically thick at these densities. Photons emitted spontaneously from the Na($3P$) atoms are reabsorbed by ground-state atoms and subsequently reemitted and reabsorbed many times before they can escape from the cell.[31] This lowers the effective radiative decay rate $\Gamma^{(\mathrm{eff})}$ below the natural rate Γ_N. However, at the densities used in this part of the experiment,[32] the collisional excitation-transfer rate for $3P_{1/2} \leftrightarrow 3P_{3/2}$ was much smaller than $\Gamma^{(\mathrm{eff})}$, so that the excited-state population created was essentially pure $3P_{1/2}$ or $3P_{3/2}$.

The energy-transfer process (1) was monitored by observing fluorescence from the $5S$, $4D$, and $3D$ states using a 3/4-meter double monochromator and a GaAs cathode photomultiplier (see Fig. 3). The density of atoms in the $nL_{J''}$ state, integrated over the observed volume, is proportional to $[\mathrm{Na}(3P_J)]^2$, integrated over the same volume. Thus, the absolute magnitude of the fluorescent intensity is very sensitive to the magnitude and distribution of $[\mathrm{Na}(3P_J)]$. However, since all of the $nL_{J''}$ states produced by process (1) have fluorescence intensities with the same dependence on $[\mathrm{Na}(3P_J)]^2$, the ratios of these intensities are therefore independent of $[\mathrm{Na}(3P_J)]^2$. Thus, in the data analysis, only intensity ratios are used.

The ratio of $5S \rightarrow 3P_{3/2}$ to $5S \rightarrow 3P_{1/2}$ fluorescence signals should be exactly 2 and this was observed within an experimental uncertainty of $\pm3\%$. To test for systematic effects such as $\mathrm{Na}(3P_J)$ velocity selection, monochromator leakage of the much stronger resonance radiation, and trapping of the $nL_{J''} \rightarrow 3P$ light by Na($3P$) atoms, and to verify that the $nL_{J''}$ intensity ratios are independent of Na($3P$) distribution, we measured the fluorescence ratios for a range of laser detunings and powers and the three sodium densities. The $nL_{J''}$ fluorescence signal ratio data from this part of the experiment are given in Fig. 4 (open and closed circles) as a function of the square root of the $5S \rightarrow 3P_{3/2}$ signal (which is proportional to $[\mathrm{Na}(3P)]$). Here, the typical uncertainty in individual ratio measurements is $\sim8\%$, and the standard deviation in the mean of all the step-(1) data in Fig. 4 is less than 4% for each signal ratio. The constancy of the observed signal versus $[\mathrm{Na}(3P)]$ gives confidence in the absence of systematic errors, such as due to radiation trapping of $nL_J \rightarrow 3P$ radiation.

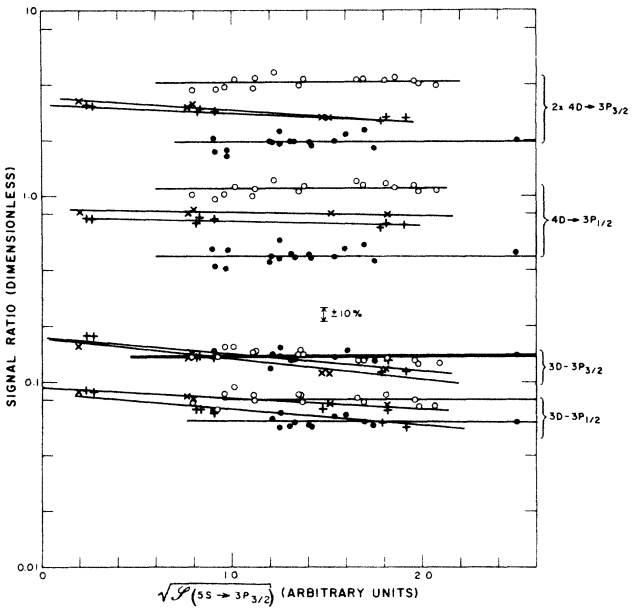

FIG. 4. Signal ratios for the indicated lines divided by the signal for $5S \rightarrow 3P_{3/2}$ vs the square root of the $5S \rightarrow 3P_{3/2}$ signal ($\mathcal{S}$) which is proportional to the Na($3P$) density. Lines are fits to the data. Part-(1) measurements with Na($3P_{1/2}$) pumping (●) and Na($3P_{3/2}$) pumping (○). Part-(3) measurements with Na($3P_{1/2}$) pumping (+) and Na($3P_{3/2}$) pumping (×). The horizontal scale should be multiplied by 10 in the latter case. To convert these signal ratios to photons/s or F ratios, multiply by 1.12 and 9.93, for $4D$ and $3D$, respectively.

B. $k_{4D}(3/2,3/2)/k_{4D}(1/2,1/2)$ data

In this part of the experiment, we excited Na($3P_{1/2}$) or Na($3P_{3/2}$) and in each case detected the total $4D \rightarrow 3P$ fluorescence. In order to obtain the ratio of $k_{4D}(3/2,3/2)$ to $k_{4D}(1/2,1/2)$ from the ratio of these two $4D \rightarrow 3P$ fluorescence intensities, we need the ratio of [Na($3P_{1/2}$)] for $D1$ pumping versus [Na($3P_{3/2}$)] with $D2$ pumping. The absorption coefficient for Na($3S_{1/2}$)→Na($3P_{1/2}$) ($D1$-line) and Na($3S_{1/2}$)→Na($3P_{3/2}$) ($D2$-line) resonance radiation differs by a factor of 2, and at the densities used here, the fundamental mode $\Gamma^{(\text{eff})}$ also differs by nearly a factor of 2 (Refs. 29 and 31) (this is a Doppler line-shape density region of Holstein's theory). Since the amount of D-line light trapping is different for the two different ($3P_{1/2}$- and $3P_{3/2}$-state) cases,[31] we must consider the possibility that the distribution of Na($3P$) atoms may also be different. To minimize any such differences, a Na density where both lines are highly trapped was used. Under those conditions, both [Na($3P_J$)] are predominantly in fundamental-mode spatial distributions, which is the same for both J states. Then, as the ratio of the $\Gamma^{(\text{eff})}$ is 2.0, the fundamental mode [Na($3P_{3/2}$)] from $D2$-line excitation will be two times the fundamental mode [Na($3P_{1/2}$)] from $D1$-line excitation if the same power is absorbed into the fundamental mode in both cases. Similarly, high-order modes will have the same shape as well as the same fractional contributions to the total density in both cases if they are excited equally. To obtain this equivalently shaped excitation for both Na($3P_{1/2}$) and Na($3P_{3/2}$), we detuned the laser so that only 10—40% of the beam was absorbed, and the excitation was nearly uniform across the 6-mm gap between the sapphire rods.

A second laser (laser No. 2 in Fig. 3), tuned to $3P_J \rightarrow 4D_{J''}$, was used to verify that the assumption that the [Na($3P_J$)] were proportional to absorbed power divided by the fundamental mode $\Gamma^{(\text{eff})}$. In order to illuminate the vapor uniformly and with low power, this second laser beam was expanded to a diameter of ~200 mm with the central portion, ~12 mm, entering the cell. We then compared the $4D_{J''} \rightarrow 3P$ fluorescence resulting from this two-step ($3S \rightarrow 3P_J \rightarrow 4D_{J''}$) optical excitation to the power absorbed from laser No. 1. As expected, this fluorescence was directly proportional to the power absorbed divided by $\Gamma^{(\text{eff})}$ for each J, and the ratio of fluorescence, [Na($3P_{3/2}$)] versus [Na($3P_{1/2}$)], was 2.0 when the same laser No. 1 power was absorbed to excite each $3P_J$ state. Also, this was done with different diameters (0.5—1.0 cm) of the laser No. 1 beam to confirm that geometric effects in the transverse direction (i.e., deviation from infinite-slab geometry) had no effect on this ratio of Na($3P_{3/2}$) to Na($3P_{1/2}$) densities. The uncertainties in these various measurements were a few percent, as the two-step fluorescence signals are quite large.

Since the sodium density and power absorbed were fairly small and since process (1) depends quadratically on Na($3P$) density, the Na($4D$) fluorescence due to energy-transfer collisions was very weak in this part of the experiment. In order to get higher light-collection efficiency with sufficient resonance-fluorescence rejection, we detected the $4D \rightarrow 3P$ fluorescence through three interference filters (in series, variously tilted to prevent multiple reflections). The residual leakage of the D-line fluorescence I_{3P}—which was $\sim 10^{10}$ times stronger than the $4D \rightarrow 3P$ fluorescence I_{4D}—was then negligible. We confirmed this by varying the power of the exciting laser light, using calibrated neutral-density filters; within ~10% uncertainty $I_{4D}/(I_{3P})^2$ was independent of laser power.

The $4D \rightarrow 3P$ fluorescence signal was measured for a factor-of-4 range in absorbed power (a factor of 16 in I_{4D}) for both Na($3P_{1/2}$) and Na($3P_{3/2}$) pumping. The measured $I_{4D}/(P_{\text{abs}})^2$ ratio did not vary systematically with P_{abs} for either Na($3P_{1/2}$) or Na($3P_{3/2}$) excitation. The ratio $I_{4D}/(P_{\text{abs}})^2$ for Na($3P_{1/2}$) versus Na($3P_{3/2}$) pumping fluctuated with a standard deviation of ~15% about a mean value of 2.76, and the standard deviation in the mean of 42 measurements was ±2.5%. The average value of 2.76 is the ratio

$$\sum_{J''} k_{4D_{J''}}(1/2,1/2) \Big/ \sum_{J''} k_{4D_{J''}}(3/2,3/2) .$$

C. $k_{nL_{J''}}(1/2,3/2)$ data

In the third part of the experiment, we raised the sodium density to $\sim 3\times 10^{14}$ cm^{-3}. At these high Na densities the $3P_{1/2} \leftrightarrow 3P_{3/2}$ excitation-transfer rate due to collisions with ground-state atoms is faster than $\Gamma^{(\text{eff})}$ for both $3P_{1/2}$ and $3P_{3/2}$ states, and [Na($3P_{3/2}$)]/[Na($3P_{1/2}$)] approaches the thermodynamic ratio of

$2\exp(\Delta E/kT)=1.92$ regardless of which state was initially populated.[32] At the actual densities we used, the $[3P_{3/2}]$/[total $3P$] ratio was 60% when pumping $3P_{1/2}$, and 69% when pumping $3P_{3/2}$, rather than the thermodynamic ratio of 66%. When the excited atoms are so mixed, about $\frac{1}{9}$ of the Na($3P$) + Na($3P$) collisions occur between Na($3P_{1/2}$) and Na($3P_{1/2}$), about $\frac{4}{9}$ between Na($3P_{1/2}$) and Na($3P_{3/2}$), and about $\frac{4}{9}$ between Na($3P_{3/2}$) and Na($3P_{3/2}$). Thus, the data from this part of the experiment contain $k_{nL_{J''}}(1/2,3/2)$, as well as $k_{nL_{J''}}(1/2,1/2)$ and $k_{nL_{J''}}(3/2,3/2)$.

The results of these measurements are shown in Fig. 4 ($\times$ and $+$), with the horizontal scale increased by a factor of 10 from that shown for step (1) since $\Gamma^{(\text{eff})}$ is now much smaller and therefore [Na($3P$)] and the excitation-transfer signals are much larger. The data in Fig. 4 should be independent of [Na($3P$)] or the horizontal position, but they exhibit some slope. These data are analyzed in Sec. III, and the anomalous slope is discussed in Sec. IV.

As noted previously, the values of the five $k_{nL_{J''}}(1/2,3/2)$ relative to $k_{n'L'_{J'''}}(3/2,3/2)$ are underdetermined by the data, and we would need accurate fluorescence ratios over a range of different ratios of [Na($3P_{3/2}$)]/[Na($3P_{1/2}$)] to determine them. However, as we discuss in the next section, the data put strong constraints on the ratios $k_{nL_{J''}}(1/2,3/2)/k_{5S}(3/2,3/2)$.

III. DATA ANALYSIS

Steady-state rate equations for the states involved in this experiment can be expressed as follows, for an arbitrary point in the cell:

$$\dot{n}_{nL_{J''}}=0=-n_{nL_{J''}}\Gamma_{nL}+\sum_{J,J'}k_{nL_{J''}}(J,J')n_{3P_J}n_{3P_{J'}}+C_{nL_{J''}}\,, \tag{2}$$

where n_{nL_J} is the local density of Na(nL_J), Γ_{nL} is the total radiative decay rate for the nL_J state, and $nL_{J''}=4D_{3/2}$, $4D_{5/2}$, $5S_{1/2}$, $4F_{5/2}$, or $4F_{7/2}$. The cascade radiation from the $3D_J$ states, used to determine the $4F_{J''}$-state rate coefficients, obeys the following equations:

$$\dot{n}_{3D_{3/2}}=0=-n_{3D_{3/2}}\Gamma_{3D}+n_{4F_{5/2}}\Gamma(4F_{5/2}\text{-}3D_{3/2})+C_{3D_{3/2}}+\sum_{J,J'}k_{3D_{3/2}}(J,J')n_{3P_J}n_{3P_{J'}}\,, \tag{3}$$

$$\dot{n}_{3D_{5/2}}=0=-n_{3D_{5/2}}\Gamma_{3D}+n_{4F_{5/2}}\Gamma(4F_{5/2}\text{-}3D_{5/2})+n_{4F_{7/2}}\Gamma(4F_{7/2}\text{-}3D_{5/2})+C_{3D_{5/2}}+\sum_{J',J}k_{3D_{5/2}}(J,J')n_{3P_J}n_{3P_{J'}}\,. \tag{4}$$

The $C_{nL_{J''}}$'s in Eqs. (2)–(4) represent radiative cascades from higher-energy states that may also be populated by Na($3P$) + Na($3P$) collisions (see Fig. 2). The states ($5S_{1/2}$, $4D_{J''}$, or $4F_{J''}$) studied in this work are those lying closest in energy (~ 630 cm^{-1}; see Fig. 2) to Na($3P_J$) + Na($3P_{J''}$) and we expect much larger rate coefficients for populating these states as compared to other states that are much further away. The next-nearest state for which exothermic excitation transfer can occur is $4P$, which is separated by ~ 3700 cm^{-1} from $2E(3P)$—thus, we expect the $4P$ state to be populated almost entirely by cascade from Na($4D$) and Na($5S$).[25] The $3D$ state is ~ 4800 cm^{-1} below Na($3P$) + Na($3P$), and we expect the $3D$ state to be populated almost entirely by cascade from Na($4F$), since 100% of $4F$ cascades to $3D$, but $<1\%$ of the $4D$ and $5S$ population radiates to $3D$. Cascading from $4P$ to $3D$ is also negligible because Na($4P$) is weakly populated and only 1.7% of $4P$ cascades to $3D$. Cascades from $5P$ are also negligible because only 0.2% radiates to $3D$.

Among the states with energies above Na($3P_J$) + Na($3P_{J'}$) that can cascade to $5S$, $4D$, and $4F$, the closest are $5P$ and $6S$ at $\Delta E_{nL}=1106$ and 2437 cm^{-1}, respectively. At our cell temperature of 640 K, $kT/hc=445$ cm^{-1}, and for these activation energies $(2L+1)\exp(-\Delta E/kT)=0.25$ for the $5P$ state, and 4.2×10^{-3} for the $6S$ state, compared to 6.3 for the $4D$ state. This gives us an upper limit of $\sim 4\%$ and $\sim 0.1\%$ for the expected size, relative to that of the $4D$ state, of the rate coefficients for populating these states. Shvegzhda *et al.*[6] have measured the rate coefficients for producing $5S$, $4D$, $5P$, $6S$, and higher states from an equilibrated mixture of Na($3P_{1/2}$) and Na($3P_{3/2}$) at a temperature similar to ours. The ratio of their $5P$ and $6S$ to $4D$ rate coefficients is $k_{5P}/k_{4D}=0.036$ and $k_{6S}/k_{4D}=1.1\times10^{-3}$, while higher states are less populated. This fits well with the above expectation based on activation energy. Since the $5P$ state branches $\sim 10\%$ to $5S$ and $\sim 2\%$ to $4D$, it produces a cascade contribution to the $5S$ state that is only $\sim 2\%$ of the direct production, and this ratio is $\ll 1\%$ for the $4D$ state. Since k_{6S} is so small, the $6S$ state produces a negligible cascading. From the activation energy argument, higher-lying states are also a negligible source of $4D$, $5S$, and $4F$ population. Thus, we can eliminate the $C_{nL_{J''}}$ from Eq. (2) for $nL=4D$, $5S$, and $4F$.

We can also neglect the $C_{3D_{J''}}$ which are due to cascades from the $5S$, $5P$, and $4D$ states (plus some of those already noted as negligible above) in Eqs. (3) and (4) as the $5S\rightarrow 4P\rightarrow 3D$, the $5P\rightarrow 3D$, and the $4D\rightarrow 4P\rightarrow 3D$ branchings are all less than 1% (see Fig. 2), and contribute a very small fraction of the observed $3D$ fluorescence. Therefore, all the cascade terms C in Eqs. (3) and (4) will be dropped. We will also assume negligible direct transfer to the $3D$ states by process (1), and drop this term from Eqs. (3) and (4). This assumption is discussed further in Sec. IV.

We have not included in the analysis any mixing of the $nL_{J''}$ states due to collisions with ground-state atoms before radiative decay. At the highest Na densities of our experiment, the rate coefficient for mixing would have to be $>10^{-6}$ cm^3/s to yield even 1% mixing before radiative decay. This rate coefficient is $\sim 10^3$ larger than typical excited-state mixing rate coefficients, so that we assume any such collisional mixing is negligible. Also, if such mixing were occurring, the data from the first step of the experiment would have shown a systematic trend versus [Na], which was not observed. Thus, we can consider any $nL_{J''}$-state population, except Na($3D_{J''}$) which is popu-

lated entirely by cascade from Na($4F_{J''}$), to be entirely due to the direct excitation-transfer reaction (1).

Defining $\mathcal{N}^2 = n_{3P_J} n_{3P_{J'}}$ and dropping the C terms we can rewrite Eq. (2) as

$$n_{nL_{J''}} = \Gamma_{nL}^{-1} \sum_{J,J'} k_{nL_{J''}}(J,J') \mathcal{N}^2(J,J') \ . \tag{5}$$

Putting Eq. (5) for the $4F$ states into Eqs. (3) and (4) yields

$$n_{3D_{3/2}} = \Gamma_{3D}^{-1} \Gamma_{4P}^{-1} \sum_{J,J'} k_{4F_{5/2}}(J,J') \mathcal{N}^2(J,J') \Gamma(4F_{5/2}\text{-}3D_{3/2}) \ , \tag{6}$$

$$n_{3D_{5/2}} = \Gamma_{3D}^{-1} \Gamma_{4F}^{-1} \sum_{J,J'} k_{4F_{5/2}}(J,J') \mathcal{N}^2(J,J') \Gamma(4F_{5/2}\text{-}3D_{5/2}) + \sum_{J,J'} k_{4F_{7/2}}(J,J') \mathcal{N}^2(J,J') \Gamma(4F_{7/2}\text{-}3D_{5/2}) \ . \tag{7}$$

In the first and third parts of the experiment, we used the ratio of detected signals, which all have the same dependence on $\mathcal{N}^2(J,J')$ in Eqs. (5)—(7). The measured intensities were obtained by dividing the signal by the instrument sensitivity, and the photon fluxes F were obtained by dividing the intensities by $h\nu$ for each detected transition. Because we image a volume within the cell, and Eqs. (5)—(7) predict the [Na($nL_{J''}$)] at a point, these equations must be integrated over the volume imaged, but the only term in the integrand which is dependent on spatial coordinates is $\mathcal{N}^2(J,J')$, and this is the same for all $nL_{J''}$ states [Eqs. (2)—(7)]. Thus, the volume integrals of $\mathcal{N}^2$ cancel when intensity *ratios* are taken. The detected photon flux is given by

$$F(nL_J\text{-}n'L'_{J'}) = \Gamma(nL_J\text{-}n'L'_{J'}) \frac{d\Omega}{4\pi} \int n_{nL_J} dV \ , \tag{8}$$

where $d\Omega/4\pi$ is the fraction of emitted light collected into the solid angle defined by our detection optics. The ratio of the detected flux signals is

$$\frac{F(nD_J\text{-}3P_{3/2})}{F(5S\text{-}3P_{3/2})} = \frac{\Gamma(nD_J\text{-}3P_{3/2}) \int n_{nD_J} dV}{\Gamma(5S\text{-}3P_{3/2}) \int n_{5S} dV} \quad \text{for } J = 3/2,\ 5/2 \text{ and } n = 3,4 \tag{9}$$

and

$$\frac{F(nD_{3/2}\text{-}3P_{1/2})}{F(5S\text{-}3P_{3/2})} = \frac{\Gamma(nD_{3/2}\text{-}3P_{1/2}) \int n_{nD_{3/2}} dV}{\Gamma(5S\text{-}3P_{3/2}) \int n_{5S} dV} \quad \text{for } n = 3,4 \ , \tag{10}$$

where the n_{nL_J} are given in Eqs. (5)—(7). Since we did not resolve the fine-structure state of the $4D$ and $3D$ levels, we add the expressions in Eq. (9) for $J=3/2$ and $J=5/2$ to obtain

$$\frac{F(nD\text{-}3P_{3/2})}{F(5S\text{-}3P_{3/2})} = \frac{\Gamma(nD_{3/2}\text{-}3P_{3/2}) \int n_{nD_{3/2}} dV + \Gamma(nD_{5/2}\text{-}3P_{3/2}) \int n_{nD_{5/2}} dV}{\Gamma(5S\text{-}3P_{3/2}) \int n_{5S} dV} \quad \text{for } n = 3,4 \ . \tag{11}$$

From Eqs. (5)—(7), in Eqs. (10) and (11), we obtain two sets of linear equations:

$$\begin{bmatrix} \frac{F(4D\text{-}3P_{1/2})}{F(5S\text{-}3P_{3/2})} \\ \frac{F(4D\text{-}3P_{3/2})}{F(5S\text{-}3P_{3/2})} \end{bmatrix} = \begin{bmatrix} \frac{B(4D_{3/2}\text{-}3P_{1/2})}{B(5S\text{-}3P_{3/2})} & 0 \\ \frac{B(4D_{3/2}\text{-}3P_{3/2})}{B(5S\text{-}3P_{3/2})} & \frac{B(4D_{5/2}\text{-}3P_{3/2})}{B(5S\text{-}3P_{3/2})} \end{bmatrix} \begin{bmatrix} \frac{k_{4D_{3/2}}(J,J')}{k_{5S}(J,J')} \\ \frac{k_{4D_{5/2}}(J,J')}{k_{5S}(J,J')} \end{bmatrix} \tag{12}$$

and

$$\begin{bmatrix} \frac{F(3D\text{-}3P_{1/2})}{F(5S\text{-}3P_{3/2})} \\ \frac{F(3D\text{-}3P_{3/2})}{F(5S\text{-}3P_{3/2})} \end{bmatrix} = \begin{bmatrix} \frac{B(4F_{5/2}\text{-}3D_{3/2})B(3D_{3/2}\text{-}3P_{1/2})}{B(5S\text{-}3P_{3/2})} & 0 \\ \frac{B(4F_{5/2}\text{-}3D_{3/2})B(3D_{3/2}\text{-}3P_{3/2}) + B(4F_{5/2}\text{-}3D_{5/2})}{B(5S\text{-}3P_{3/2})} & \frac{1}{B(5S\text{-}3P_{3/2})} \end{bmatrix} \begin{bmatrix} \frac{k_{4F_{5/2}}(J,J')}{k_{5S}(J,J')} \\ \frac{k_{4F_{5/2}}(J,J')}{k_{5S}(J,J')} \end{bmatrix} , \tag{13}$$

where the branching fractions B are

$$B(nL_J\text{-}n'L'_{J'}) = \frac{\Gamma(nL_J\text{-}n'L'_{J'})}{\Gamma_{nL}} \ .$$

These equations can be inverted to relate the measured flux ratios $F(nD\text{-}3P_J)/F(5S\text{-}3P_J)$ to the desired ratios of rate coefficients. The values of the branching factors $B(nL_J\text{-}n'L'_{J'})$ obtained from Ref. 33 and sum rules are given in Table I.

In the first experimental step, where only $3P_{1/2}$ or $3P_{3/2}$ was excited (see Sec. II A), Eqs. (12) and (13) yield $k_{nL_{J''}}(J,J)/k_{5S}(J,J)$ for $J=1/2$ or $3/2$. The data were also analyzed with the inclusion of the cascade terms $C_{nL_{J''}}$ from Eqs. (3) and (4), and it was found that their contribution was indeed negligible (less than or approximately equal to 1% for all but $k_{4F_{5/2}}$, where $4D$ and $5S$ cascading to $3D$ had $\sim 5\%$ effect). The results of the data analysis from step (1) are given in Table II. Note

TABLE I. Branching fractions used in this work.[a]

nL_J	$n'L'_{J'}$	$B(nL_J\text{-}n'L'_{J'})$
$4D_{3/2}$	$3P_{3/2}$	0.11
$4D_{3/2}$	$3P_{1/2}$	0.55
$4D_{5/2}$	$3P_{3/2}$	0.66
$3D_{3/2}$	$3P_{3/2}$	0.17
$3D_{3/2}$	$3P_{1/2}$	0.83
$3D_{5/2}$	$3P_{3/2}$	1.00
$4F_{5/2}$	$3D_{5/2}$	0.067
$4F_{5/2}$	$3D_{3/2}$	0.93
$4F_{7/2}$	$3D_{5/2}$	1.00
$5S_{1/2}$	$3P_{3/2}$	0.38
$5S_{1/2}$	$3P_{1/2}$	0.19
$5P_{3/2}$	$5S_{1/2}$	0.50
$5P_{1/2}$	$5S_{1/2}$	0.50
$\sum_J 4P_J$	$\sum_{J'} 3D_{J'}$	0.017
$\sum_J 5P_J$	$\sum_{J'} 4D_{J'}$	0.022

[a]Taken from Ref. 33 and sum rules.

that the ratios appearing in the two rows in the table apply within each row only, not between rows. Sources of uncertainty in the rate-coefficient ratios in Table II are uncertainty in branching ratios (10% for $5S$, 5% for $4D$, 0% for $4F$), uncertainty in monochromator plus photomultiplier sensitivity versus wavelength ($\sim$7%), and statistical uncertainties (2–3%). The only significant cascade uncertainty is $\sim$5% for $4F$. The net uncertainty is thus $\sim$10% for all ratios. To establish the relationship between the two rows is the next objective.

In the second experimental step (see Sec. II B), we compared $4D\rightarrow 3P$ fluorescence from both J'' states produced by collisions between two Na($3P_{3/2}$) atoms with the $4D\rightarrow 3P$ fluorescence due to collisions between two Na($3P_{1/2}$) atoms. Since we used interference filters in this part of the experiment, we did not resolve the two $4D\rightarrow 3P_J$ lines, so the observed fluorescence is a measure of the total rate coefficient $k_{4D}=k_{4D_{3/2}}+k_{4D_{5/2}}$. By comparing the fluorescence intensity in the two D-line pumping schemes, we obtained $k_{4D}(3/2,3/2)/k_{4D}(1/2,1/2)$. The total, volume-integrated rate of excitation transfer R to both Na($4D$) fine-structure states can be expressed as $R_{4D}(J,J')=R_{4D_{3/2}}(J,J')+R_{4D_{5/2}}(J,J')$, which from Eq. (5) equals

$$R_{4D}(J,J')=k_{4D}(J,J')\int\mathcal{N}^2(J,J')dV\ , \tag{14}$$

where $k_{4D}(J,J')=k_{4D_{3/2}}(J,J')+k_{4D_{5/2}}(J,J')$. Thus the ratio of the measured intensities equals

$$\frac{R_{4D}(3/2,3/2)}{R_{4D}(1/2,1/2)}=\frac{k_{4D}(3/2,3/2)}{k_{4D}(1/2,1/2)}\frac{\int\mathcal{N}^2(3/2,3/2)dV}{\int\mathcal{N}^2(1/2,1/2)dV}\ . \tag{15}$$

For the same absorbed power of $D1$ versus $D2$ radiation and small laser-beam attenuation,

$$\frac{\int\mathcal{N}^2(3/2,3/2)dV}{\int\mathcal{N}^2(1/2,1/2)dV}=\left[\frac{\Gamma^{(\mathrm{eff})}_{3P_{3/2}}}{\Gamma^{(\mathrm{eff})}_{3P_{1/2}}}\right]^2\ . \tag{16}$$

At the sodium densities we used, Holstein's theory of radiation trapping[31] predicts (in the Doppler regime) $\Gamma^{(\mathrm{eff})}_{3P_{3/2}}/\Gamma^{(\mathrm{eff})}_{3P_{1/2}}=2.00$, and we have verified this using the second laser, as described in Sec. II B. Therefore, from the measured $4D\rightarrow 3P$ intensity ratio, $R_{4D}(3/2,3/2)/R_{4D}(1/2,1/2)=2.76$ reported in Sec. II B. From this and the ratio of $\Gamma^{(\mathrm{eff})}$'s we find that $k_{4D}(3/2,3/2)/k_{4D}(1/2,1/2)=2.76/2^2=0.69$. From the $k_{4D}(J,J)/k_{5S}(J,J)$ in Table II for $J=1/2$ and $J=3/2$ this yields $k_{5S}(1/2,1/2)/k_{5S}(3/2,3/2)=3.2$. This factor multiplying the first row of Table II yields the ratios of rate coefficients in the two rows. The result is given in Table III, with all ratios given relative to $k_{5S}(3/2,3/2)$.

The standard deviation in the mean from this part of the experiment, relating the first and second rows of Table II, was $\sim$2.5%. Allowing for the possibility of systematic effects not seen in the much more scattered individual measurements, we consider 10% a reasonable uncertainty. This is added in quadrature with the uncertainties from the first step to yield the uncertainties listed in Table III.

In the third stage of the experiment, at much higher [Na] where a nearly equilibrated mixture of Na($3P$) population occurs, the measured excitation transfer to each $nL_{J''}$ is a weighted average of the excitation transfer from the three (J,J') combinations of $(J,J')=(1/2,1/2)$, $(1/2,3/2)$, $(3/2,3/2)$, with a weighting, $P(J,J')$, of approximately $\frac{1}{9}$, $\frac{4}{9}$, and $\frac{4}{9}$, respectively. Thus, the effective rate coefficient can be written as

$$k^{(\mathrm{eff})}_{nL_{J''}}=\sum_{J=1/2,J'=3/2}k_{nL_{J''}}(J,J')P(J,J')\ .$$

Thus we define a ratio of effective rate coefficients as $r_{nL_{J''}}=k^{(\mathrm{eff})}_{nL_{J''}}/k^{(\mathrm{eff})}_{5S}$:

$$r_{nL_{J''}}=\frac{\sum_{J,J'}k_{nL_{J''}}(J,J')P(J,J')}{\sum_{J,J'}k_{5S}(J,J')P(J,J')}\ , \tag{17}$$

where $P(J,J')$ is the fraction of the total Na($3P$) + Na($3P$) collisions involving Na($3P_J$) + Na($3P_{J'}$). The

TABLE II. Ratio of rate coefficient $k_{nL_{J''}}(J,J)$ relative to $k_{5S}(J,J)$. Uncertainties are $\approx$10%—see text for detailed explanation.

J	$4D_{3/2}$	$4D_{5/2}$	$4F_{5/2}$	$4F_{7/2}$
1/2	0.39	0.61	0.30	0.46
3/2	0.91	1.3	0.39	0.44

TABLE III. Ratios $K_{nL_J}(J,J)$ [rate coefficients relative to $k_{5S}(3/2,3/2)$; see Eq. (19)]. Uncertainties are $\approx$15% for $J=1/2$, $\approx$10% for $J=3/2$.

J	$5S_{1/2}$	$4D_{3/2}$	$4D_{5/2}$	$4F_{5/2}$	$4F_{7/2}$
1/2	3.2	1.3	1.9	0.96	1.4
3/2	1	0.91	1.3	0.39	0.44

terms $k_{nL_{J''}}(J,J)$ in Eq. (17) are known from the first and second parts of the experiment, and there are five k values to be determined, but only four measured ratios $r_{nL_{J''}}$.

As noted above, the $k_{nL_{J''}}(1/2,3/2)$ are underdetermined by the present experiment, but we can use the results from Table III and the $r_{nL_{J''}}$ measurements to put constraints on the $k_{nL_{J''}}(1/2,3/2)$. By inverting Eq. (17) we arrive at the following four linear relations for $nL_{J''}=4D_{3/2}$, $4D_{5/2}$, $4F_{5/2}$, and $4F_{7/2}$:

$$K_{nL_{J''}}(1/2,3/2)=r_{nL_{J''}}K_{5S}(1/2,3/2)+Z_{nL_{J''}}\ , \tag{18}$$

where we have defined

$$K_{nL_{J''}}(J,J')\equiv\frac{k_{nL_{J''}}(J,J')}{k_{5S}(3/2,3/2)} \tag{19}$$

and

$$Z_{nL_{J''}}=\frac{[r_{nL_{J''}}K_{5S}(1/2,1/2)-K_{nL_{J''}}(1/2,1/2)]P(1/2,1/2)+[r_{nL_{J''}}-K_{nL_{J''}}(3/2,3/2)]P(3/2,3/2)}{P(1/2,3/2)}\ . \tag{20}$$

The terms $K_{nL_{J''}}(J,J)$ were determined in steps (1) and (2) of the experiment and appear in Table III. The $r_{nL_{J''}}$ are the measured photon flux ratios from this part of the experiment, and the $P(J,J')$ are known. Therefore, the $Z_{nL_{J''}}$ are known and are given in Table IV along with values for $P(J,J')$. Thus, Eq. (18) provides a linear relationship among the five $k_{nL_{J''}}$. Plots of $K_{nL_{J''}}(1/2,3/2)$ as a function of $K_{5S}(1/2,3/2)$ [from Eq. (18)] appear in Fig. 5, which is discussed below.

IV. DISCUSSION

There is a great variety of theoretical and experimental information on Na_2 potential curves (see Ref. 34 for all Na studies up to 1983 and Refs. 19 and 13 for recent calculations). However, most of these are for a lower energy region than of interest here, with the exception of Rydberg states, which do not reach the large R region (R the internuclear distances) of interest here. Kowalczyk[16–18] has calculated the Na_2 potentials for Na(3P) + Na(3P) and Na(4D) + Na(3S) in our region of interest. Kowalczyk has not explicitly treated the J dependence of the states that he has calculated, nor has he included the Na(4F) + Na(3S) or Na(5S) + Na(3S) states. Allegrini *et al.*[13] have included the 4F and 5S states but they do not treat the J dependence. Henriet *et al.*[19] have some of the calculated Na_2 potentials in this region; however, they do not address the issue of excitation transfer to the $nL_{J''}$ states, nor the fine structure.

TABLE IV. r_{nL_J} is the ratio of rates of production relative to rate of 5S production, $P(J,J')$ is the fraction of collisions between Na(3P_J) and Na(3$P_{J'}$) atoms. See text for definition of $Z_{nL_{J''}}$.

State pumped	$3P_{1/2}$	$3P_{3/2}$
$P(1/2,1/2)$	0.16	0.097
$P(1/2,3/2)$	0.48	0.43
$P(3/2,3/2)$	0.36	0.47
$r_{4D_{3/2}}$	0.62	0.73
$r_{4D_{5/2}}$	0.92	0.97
$r_{4F_{5/2}}$	0.39	0.42
$r_{4F_{7/2}}$	0.50	0.45
$Z_{4D_{3/2}}$	0.00	0.03
$Z_{4D_{5/2}}$	0.04	−0.10
$Z_{4F_{5/2}}$	0.09	0.11
$Z_{4F_{7/2}}$	0.09	0.02

The $Na^+ + Na^-$ ion-pair potential crosses the region of the Na(3P) + Na(3P) potential at $R\sim 40$ Å. At this very large separation, electron transfer is very unlikely, so that hopping to the ion-pair state probably does not play a significant role in the excitation-transfer process (1).

The uncertainties in J'' dependences of $k_{nL_{J''}}$ are only 2–3 % since only the statistical uncertainties effect these. The $k_{4D_{J''}}(1/2,1/2)$ are in the ratio of their statistical weights $2J''+1$, as are the $k_{4D_{J''}}(3/2,3/2)$. One possible explanation of this is that considerable nonadiabatic mixing may be taking place in the fine-structure recoupling region as the quasimolecule separates to the dissociated state Na(4$D_{J''}$) + Na(3$S_{1/2}$). For the 4F case, the statistical ratio is 1.5 and we observe 1.33 and 1.13, respectively, for $J=1/2$ and 3/2.

Also note that k_{4D}/k_{4F} equals 1.36 and 2.7 for $J=1/2$ and 3/2 whereas the ratio of statistical weights equals 5/7. This argues against complete mixing of 4D and 4F states during separation, although they are only separated by 38 cm^{-1}.

When the values for the five ratios of rate coefficients [all relative to $k_{5S}(3/2,3/2)$] in each row of Table III are compared, it is seen that there are large variations. This is another noteworthy result relating to state-specific coupling. It indicates that the Na(3P_J) + Na(3$P_{J'}$) population tends to follow adiabatic states as the atoms pass through the fine-structure recoupling region. They then pass into the smaller R region where avoided crossings with states of Na($nL_{J''}$) + Na(3S) parentage result in transfer to particular $nL_{J''}$ states.

Symmetry plays an important role in determining the Landau-Zener hopping probability at avoided crossings. Because there are so many states involved in reaction (1), the calculation of the potential-curve hopping and the tracing of an atom along the tortuous path through the manifold of these states' potential curves will be difficult, even once the adiabatic potentials are known. Thus, it is difficult to draw specific conclusions as to which initial

state will result in which final state. One possible exception is the state that separates to Na($5S$) + Na($3S$), which should be favored from Na($3P_{1/2}$) + Na($3P_{1/2}$). This is expected because the Na($3P_{1/2}$) + Na($3P_{1/2}$) states have the lowest energy at large R, and as the manifold of Na($3P_J$) + Na($3P_{J'}$) states fan out with decreasing R, the Na ($3P_{1/2}$) + Na($3P_{1/2}$) will stay adiabatically in the lowest-energy state. Na($5S$) + Na($3S$) is below Na($3P$) + Na($3P$) (see Fig. 1), so this causes a greater propensity for Na($3P_{1/2}$) + Na($3P_{1/2}$) to cross Na($5S$) + Na($3S$). A second reason for a large $k_{5S}(1/2,1/2)$ is that the Na($3P_{1/2}$) + Na($3P_{1/2}$) states form mostly an $\Omega=0$ state, as do the Na($5S$) + Na($3S$) states, so that these are strongly coupled in the crossing region. These states also have the same symmetry in the j-j coupling scheme. Therefore, it is no surprise that $k_{5S}(1/2,1/2)$ is 3.2 times larger than $k_{5S}(3/2,3/2)$.

In the case of the Na($3P_{1/2}$) + Na($3P_{3/2}$) data the measured flux ratios lie between the corresponding ratios for Na($3P_{1/2}$) + Na($3P_{1/2}$) collisions and Na($3P_{3/2}$) + Na($3P_{3/2}$) collisions (see Fig. 4). This suggests [see Eq. (17)] that the rate coefficients are also so ordered—i.e., $k_{nL_{J''}}(1/2,1/2) > k_{nL_{J''}}(1/2,3/2) > k_{nL_{J''}}(3/2,3/2)$ for all the $nL_{J''}$. If one assumes that $K_{5S}(1/2,3/2)$ is about equal to the arithmetic and geometric means between $K_{5S}(1/2,1/2)$ and $K_{5S}(3/2,3/2)$, then $K_{5S}(1/2,3/2)\simeq 1.9$. Then from Fig. 5, where this is indicated as a vertical dashed line, the measurements yield $K_{nL_{J''}}(1/2,3/2)\cong 1.2$, 1.8, 0.8, and 1.0 for $nL_{J''}=4D_{3/2}$, $4D_{5/2}$, $4F_{5/2}$, and $4F_{7/2}$, respectively. As seen in Fig. 5, which is a plot of Eq. (18), all but one of these $K_{nL_{J''}}(1/2,3/2)$ lie between the corresponding $K_{nL_{J''}}(1/2,1/2)$ and $K_{nL_{J''}}(3/2,3/2)$, which are indicated as horizontal dashed lines. Thus, the data are consistent with $k_{nL_{J''}}(1/2,3/2)$ being approximately between $k_{nL_{J''}}(1/2,1/2)$ and $k_{nL_{J''}}(3/2,3/2)$.

In the mixed population data of Fig. 4 ($\times$ and $+$), there appears to be a slope that exceeded the experimental uncertainty in this plot against [Na($3P$)], by about a factor of 3 in the $4D\rightarrow 3P_{3/2}$, $3D\rightarrow 3P_{3/2}$, and $3D\rightarrow 3P_{1/2}$ data and a factor of 2 in the $4D\rightarrow 3P_{1/2}$ data. Here the uncertainty in individual measurements ranging from 8% to 40% for the various states is much less than the variation between the lowest and highest signal data. This should not occur, and it does not appear in the other data in Fig. 4 taken at a much lower [Na($3P$)]. We have considered many possible causes of this, and some of these are discussed in the paragraphs which follow.

At the right side of Fig. 4, [Na($3P$)] is sufficient to cause some radiation trapping of the $3D$-$3P$ fluorescence, but much less trapping of $4D$-$3P$ and $5S$-$3P$ fluorescence. The primary effect of this $3D$-$3P$ light trapping should be to redistribute the $3D$-$3P_J$ fluorescence between the $J=1/2$ and $J=3/2$ components. However, this effect is not seen in the data of Fig. 4, implying that such trapping was relatively minor. Another effect of such trapping is to redistribute the region of Na($3D$) density more evenly throughout the cell, thereby decreasing the intensity in the slit-image observed region. We do not think this could produce the size of the effect seen in Fig. 4, as the detected region is finite in width. The larger slopes in the $3D$ data does, however, fit this qualitatively. But since the absorption coefficient of $4D$-$3P$ is $\frac{1}{10}$ that of $3D$-$3P$, we feel that trapping of $nL_{J''}\rightarrow 3P$ radiation is not an adequate explanation for the slope.

Velocity selection of the Na($3P$) atoms by the laser detuning might be a cause. However, this is unlikely since the $3S$-$3P$ light is so highly trapped and most atoms are excited by spectrally redistributed, diffusing radiation. Most of the resonance light reaching the cell's interior was reradiated light and therefore not capable of velocity selection. We can also rule out laser power effects since tests were made with neutral-density filters, included in the data in Fig. 4, and these showed the same effect as we saw obtaining the same $F(5S$-$3P_{3/2})$ by detuning.

We can also rule out collisional mixing of the $4D$ and $4F$ states by any species, because the mixing of these would give them opposite slopes—as one is depleted, the other is filled. Further, we can rule out the quenching of the $nL_{J''}$ states by collisions with electrons or Na($3P$) atoms (Ref. 7 discusses this process for potassium). Mixing by electrons seems to be an unlikely explanation since $4D\leftrightarrow 4F$ mixing should be much faster than energy transfer to other states, and we see no evidence of this

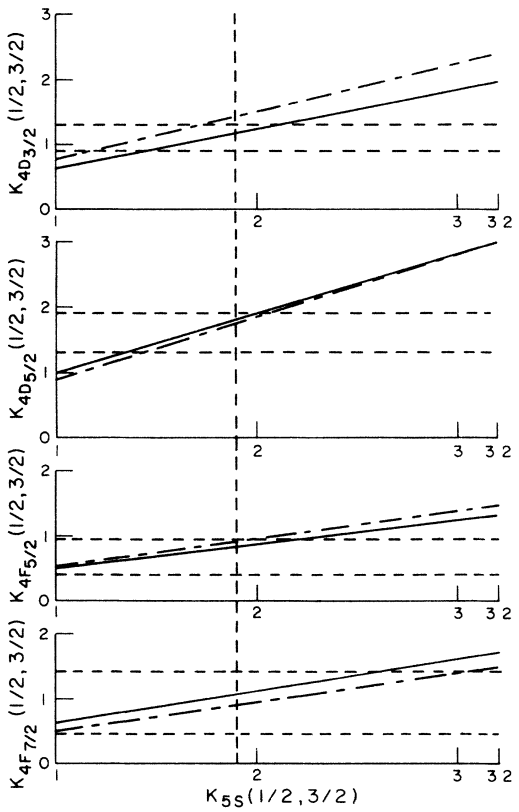

FIG. 5. Plots of the measured $K_{nL_{J''}}(1/2,3/2) = k_{nL_{J''}}(1/2,3/2)/k_{5S}(3/2,3/2)$ as a function of $K_{5S}(1/2,3/2) = k_{5S}(1/2,3/2)/k_{5S}(3/2,3/2)$ which is unknown [see Eq. (15)]. Solid lines represent the results for Na($3P_{1/2}$) pumping; slanted dashed lines for Na($3P_{3/2}$) pumping. Horizontal dashed lines are $K_{nL_{J''}}(1/2,1/2)$ and $K_{nL_{J''}}(3/2,3/2)$ (upper and lower, respectively), and vertical dashed line is at $k_{5S}(1/2,3/2)=1.9$ (see text).

mixing (again since the slopes have the same sign). The Na($3P$) density is too small to yield significant collisions with Na($nL_{J''}$) in τ_{nL}.

Leakage of the bright $3P \rightarrow 3S$ fluorescence into the photomultiplier can also be ruled out as a cause of this slope. Often in experiments, the weaker-signal data are "contaminated" by leakage of more intense light. However, the data for this experiment were taken by scanning the monochromater through the lines, thereby allowing us to subtract off background and leakage.

One possible explanation is photoionization of $nL_{J''}$ states by the D-line laser light (a process originally noted by Lucatorto and McIlrath[22]). As the laser is tuned closer to resonance, the number of trapped photons (the x axis in Fig. 4), and also the population of Na($3P$), builds up. Smith *et al.*[35] report that the ionization cross section in their experiment, where the wavelength was about twice that used here, is ten times larger for Na($4D$) than for Na($5S$). However, the photoionization cross sections from their work are about 3 orders of magnitude too small than is necessary to sufficiently photoionize a few percent of the $nL_{J''}$ states within τ_{nL}, and smaller cross sections are expected at 590 nm. We have also been unable to think of a means by which the very small Na_2 concentration in the experiment could cause this effect.

In conclusion, there might be an unknown effect proportional to [Na($3P$)], or we may not have considered all of the ramifications of $nL_{J''} \rightarrow 3P$ radiation trapping, so that the left-axis extrapolation in Fig. 4 could be correct. Since we cannot explain the mechanism for the slope we have taken an average of the left-axis extrapolation with the mean of the measurements.

It is worth noting that the significant direct populating of Na($3D$) by process (1) appears unlikely. The cross section for populating the $4D$ state reported by Huennekens and Gallagher[3] from a mixture of the $3P_{1/2}$ and $3P_{3/2}$ states is 23 Å^2, and from Table III the cross section to $4F$ is about $\frac{2}{3}$ of this, corresponding to an internuclear distance of 2.7 Å. The energy difference, $\Delta E_{nL} = E_{nL} - 2E_{3P}$, for $4D$ is 613 cm^{-1}, whereas ΔE_{3D} is -4763 cm^{-1} or -0.6 eV. Therefore, for the Na($3P$) + Na($3P$) and Na($3D$) + Na($3S$) potentials to be perturbed enough to approach one another, the internuclear distance must be very small, and that is highly unlikely since the excitation transfer [process (1)] to the nL states studied in this experiment is a long-range effect, and would occur, during a collision, long before excitation transfer to the $3D$ state could occur.

The mixed population rates $r_{nL_{J''}}$ could be turned into absolute rate coefficients if an absolute measurement of the rate coefficient for one of the $nL_{J''}$ states were known for a collision between Na($3P_{1/2}$) and Na($3P_{3/2}$). However, no experiment to date has measured this, which would have required precise determination of [Na] over a range of densities. Our results, along with those of Huennekens and Gallagher,[3] might have provided this; however, the large uncertainties in both density measurements and their rate coefficients would make any result meaningless.

Very recently Allegrini *et al.*[13] have reported a measurement of the k_{4F}/k_{4D} ratio which, under their $D2$-pumping conditions, is the ratio $k_{4F}(3/2,3/2)/k_{4D}(3/2,3/2)$. Their value for this ratio is 0.18 ± 0.09 at $T \sim 530$ K, whereas the results reported here give 0.38 ± 0.06 at $T = 640$ K. As $\Delta E_{4D} \cong \Delta E_{4F}$, the difference in temperature cannot account for the discrepancy on the basis of activation energy. There is no other experimental information on a possible temperature dependence to k_{4F}/k_{4D}, but it appears unlikely that the 20% temperature difference can explain the factor-of-2 disagreement in the measurements.

The Na density used by Allegrini *et al.* was similar to those reported here, but they detected infrared fluorescence from the $4D$ and $4F$ states and, due to the much lower sensitivity of infrared detectors, they worked with laser-beam intensities approximately 200 times larger than we used. At these higher Na($3P$) densities and light intensities, higher-order processes are much more likely, and indeed some were observed in Ref. 13 in a He-buffered cell. As expected and as confirmed by our measurements versus laser intensity and excited-atom density, these higher-order processes were insignificant in our experiment.

If significant trapping of the $4D \rightarrow 3P$ radiation occurred in the experiment of Allegrini *et al.*[13] this could explain much of the discrepancy between the reported $k_{4F}(3/2,3/2)/k_{4D}(3/2,3/2)$ ratios. Such trapping would cause an increase in the observed $I_{4D \rightarrow 4P}$ fluorescence at the expense of $I_{4D \rightarrow 3P}$, i.e., the effective branching of the $4D$ state into the observed $I_{4D \rightarrow 4P}$ fluorescence becomes $\Gamma_{4D \rightarrow 4P}/(\Gamma_{4D \rightarrow 4P} + \Gamma^{(\text{eff})}_{4D \rightarrow 3P})$, and $\Gamma^{(\text{eff})}_{4D \rightarrow 3P}$ decreases due to radiation trapping. From the intensities used by Allegrini *et al.* we estimate the Na($3P$) density is sufficient to cause significant $4D \rightarrow 3P$ radiation trapping in their experiment, although we cannot be quantitative without the exact parameters necessary for this calculation. Such an effect would appear as a negative slope in their Fig. 4, which is not inconsistent with the reported data.

From the brief experimental description in Allegrini *et al.*,[13] we cannot establish if they eliminated the wavelength dependence of imaging the small, optically excited region into their monochromator slit. That this could be a problem in their experiment is indicated by the reported $I_{4P \rightarrow 4S}/I_{4S \rightarrow 3P}$ ratio (2.3/2.9 in Table I of Ref. 13) which should equal $\lambda_{4S \rightarrow 3P}/\lambda_{4P \rightarrow 4S}$ because these lines come from a cascade transition and must represent the same number of photons (the $5P \rightarrow 4S$ line is of negligible intensity in their Fig. 3). However, the reported intensity ratio is 1.54 times the wavelength ratio, suggesting a problem with some part of the optical collection system.

In order to measure k_{4F}/k_{4D}, Allegrini *et al.* measured the ratio I_{4F}/I_{4D} of infrared fluorescence from the $4D$ and $4F$ states for a range of Na densities or temperatures, and observed changes in the ratio which they attributed to Na($4D$)↔Na($4F$) mixing by collisions with Na($3S$) atoms. A mixing rate coefficient of $k \sim 10^{-8}$ cm^3/s^{-1} between these levels (separated by 38 cm^{-1}) was necessary to explain the data. This rate coefficient is an order of magnitude larger than that for mixing the two Na($3P_J$) states,[32] which are coupled by the long-range resonant dipole interaction and are 17 cm^{-1} apart, casting considerable doubt on this interpretation. We believe that the correct explanation of their observed I_{4F}/I_{4D} variation (see Fig. 4

of Ref. 30) is $Na(3P_{1/2}) \leftrightarrow Na(3P_{3/2})$ collisional mixing which occurs at the higher sodium densities, i.e., the change in I_{4D}/I_{4F} is due to the transition from $NA(3P_{3/2}) + Na(3P_{3/2})$ collisions to collisions between a mixture of $Na(3P_{1/2})$ and $Na(3P_{3/2})$ atoms. We have measured 0.38 for the former case and $k_{4F}/k_{4D} \rightarrow 0.55 \pm 0.05$ as $[Na(3P_{3/2})]/[Na(3P_{1/2})]$ approaches a statistical ratio (this transition occurs in our 0.63-cm-wide cell at $[Na] \sim 10^{14}$ cm^{-3}). The $Na(3P_J)$ fine-structure mixing should occur before $4D \leftrightarrow 4F$ mixing because the $3P_J$ mixing rate competes with the much slower $\Gamma^{(eff)}$ (due to resonance radiation trapping), whereas the $Na(4D) \leftrightarrow Na(4F)$ mixing competes with the faster natural radiative decay rates Γ_N for $Na(4D)$ and $Na(4F)$. From our present understanding of the excited-atom geometry in Ref. 13, we expect a fraction of this $\sim 50\%$ increase (from 0.38 to 0.55) in k_{4F}/k_{4D} to occur in their experiment, explaining their observed variation with temperature.

V. SUMMARY

We have determined relative values for the rate coefficient $k_{nL_{J''}}(J,J')$ when $J = J' = 1/2$ and $3/2$ for $nL_{J''} = 5S_{1/2}$, $4D_{3/2}$, $4D_{5/2}$, $4F_{5/2}$, and $4F_{7/2}$. These ten values which appear in Table III and data from a mixture of $Na(3P_{1/2})$ and $Na(3P_{3/2})$ atoms were then used to determine to within one parameter the five remaining rate coefficients for $J = 1/2$, $J' = 3/2$ collisions (Table IV). In the literature at this time, there are no papers reporting rate coefficients for anything but a (nearly) equilibrated mixture of $Na(3P)$ [or a pure $Na(3P_J)$ population]. These papers do not separate out the contribution of the $Na(3P_{1/2}) + Na(3P_{3/2})$ to the rate in process (1), which is the one parameter needed to complete the set.

When all 15 relative rate coefficients have been determined, their comparison with the absolute measurements of the rate coefficients made by Allegrini *et al.*[2] will make possible the absolute determination of these 15 rate coefficients.

ACKNOWLEDGMENTS

The authors gratefully acknowledge A. V. Phelps and C. V. Kunasz for useful discussions. This work was supported in part by National Science Foundation Grant No. PHY82-00805 through the University of Colorado.

*Present address: Time and Frequency Division, National Bureau of Standards, Boulder, CO 80303.

†Also at Quantum Physics Division, National Bureau of Standards, Boulder, CO 80309.

[1] M. Allegrini, G. Alzetta, A. Kopystynska, and L. Moi, Opt. Commun. **19**, 96 (1976).

[2] M. Allegrini, P. Bicchi, and L. Moi, Phys. Rev. A **28**, 1338 (1983).

[3] J. Huennekens and A. Gallagher, Phys. Rev. A **27**, 771 (1983).

[4] V. S. Kushawaha and J. J. Leventhal, Phys. Rev. A **22**, 2468 (1980).

[5] V. S. Kushawaha and J. J. Leventhal, Phys. Rev. A **25**, 570 (1982).

[6] Zh. L. Shvegzhda, S. M. Papernov, and M. L. Janson, Chem. Phys. Lett. **101**, 187 (1983).

[7] M. Allegrini, S. Gozzini, I. Longo, P. Savino, and P. Bicchi, Nuovo Cimento **1D**, 49 (1982).

[8] S. G. Leslie, J. T. Verdeyen, and W. S. Millar, J. Appl. Phys. **48**, 4444 (1977).

[9] L. Barbier and M. Chéret, J. Phys. B **16**, 3213 (1983).

[10] A. N. Klyucharev and A. V. Lazarenko, Opt. Spektrosk. **32**, 1063 (1972) [Opt. Spectrosc. (USSR) **32**, 576 (1972)].

[11] This paper describes the reverse process. T. Yabuzaki, A. C. Tam, M. Itou, W. Happer, and S. M. Curry, Opt. Commun. **24**, 305 (1978).

[12] V. M. Borodin and I. V. Kamarov, Opt. Spektrosk. **36**, 250 (1974) [Opt. Spectrosc. (USSR) **36**, 145 (1974)].

[13] M. Allegrini, C. Gabbanini, L. Moi, and R. Colle, Phys. Rev. A **32**, 2068 (1985).

[14] E. E. Nikitin, *Theory of Elementary Atomic and Molecular Processes in Gases* (Clarendon, Oxford, 1974).

[15] M. S. Child, *Molecular Collision Theory* (Academic, New York, 1974).

[16] P. Kowalczyk, Chem. Phys. Lett. **68**, 203 (1979).

[17] P. Kowalczyk, Chem. Phys. Lett. **74**, 80 (1980).

[18] P. Kowalczyk, J. Phys. B **17**, 817 (1984).

[19] A. Henriet, F. Masnou-Seeuws, and C. LeSech, Chem. Phys. Lett. **118**, 507 (1985).

[20] W. Müller and I. V. Hertel, Appl. Phys. **24**, 33 (1981).

[21] W. Müller, J. J. McClelland, and I. V. Hertel, Appl. Phys. B **31**, 131 (1983).

[22] T. B. Lucatorto and T. J. McIlrath, Appl. Opt. **19**, 3948 (1980).

[23] D. J. Krebs and L. D. Schearer, J. Chem. Phys. **75**, 3340 (1981).

[24] B. Carré *et al.*, Opt. Commun. **52**, 29 (1984).

[25] F. Roussel, P. Breger, G. Spiess, C. Manus, and S. Geltman, J. Phys. B **12**, L631 (1980).

[26] R. M. Measures, J. Appl. Phys. **48**, 2673 (1977).

[27] T. Stacewitz, Opt. Commun. **35**, 239 (1980).

[28] M. Allegrini, W. P. Garver, V. S. Kushawaha, and J. J. Leventhal, Phys. Rev. A **28**, 199 (1983).

[29] J. Huennekens and A. Gallagher, Phys. Rev. A **28**, 238 (1983).

[30] J. P. Huennekens, Ph.D. thesis, University of Colorado, 1982.

[31] T. Holstein, Phys. Rev. **72**, 1212 (1947); **83**, 1159 (1951).

[32] J. Huennekens and A. Gallagher, Phys. Rev. A **27**, 1851 (1983).

[33] W. L. Wiese, M. W. Smith, and B. M. Miles, *Atomic Transition Probabilities*, Natl. Bur. Stand. Ref. Data Ser., Natl. Bur. Stand. (U.S.) Circ. No. 22 (U.S. GPO, Washington, D.C., 1969), Vol. II.

[34] K. K. Verma, J. T. Bahns, A. R. Rajaei-Rizi, W. C. Stwalley, and W. T. Zemke, J. Chem. Phys. **78**, 3599 (1983).

[35] A. V. Smith, J. E. M. Goldsmith, D. E. Nitz, and S. J. Smith, Phys. Rev. A **22**, 577 (1980).